Pergamon

Journal of Structural Geology, Vol. 17, No. 12, pp. 1785 to 1788, 1995

0191-8141/95 $9.50+0.00

0191-8141(95)00077-1

Brevia

SHORT NOTES

A method for quantifying the kinematics of fault-bend folding

STUART HARDY

Institute of Earth Sciences (Jaume Almera), Consejo Superior de Investigaciones Cientificas (CSIC), Martí i Franquès s/n, 08028 Barcelona, Spain

(*Received* 17 *March* 1995; *accepted in revised form* 28 *June* 1995)

Abstract—A Eulerian velocity description of deformation and a block contact condition are used to quantify the kinematics of fault-bend folding. The orientations of active axial surfaces (velocity boundaries) and the changes in slip necessary across them can be quantified using this approach. The method is general and includes previous geometric models of fault-bend folding.

INTRODUCTION

Since the concept was first introduced by Rich (1934), fault-bend folding has been the subject of much research (Suppe 1983, Zoetemeijer *et al.* 1992). In recent years, considerable effort has focused upon geometric modelling of such structures (Suppe 1983, Suppe *et al.* 1991) and on the relationship between fold growth and sedimentation (Hardy & Poblet 1995). The majority of these studies have been based on the geometric model of Suppe (1983) which describes the relationship between fault-shape, fold-shape and slip for both simple and complex fault-bend folds. For a simple step in décollement fault-bend fold, these relationships are:

$$\tan \theta = \sin 2\gamma/(2\cos^2 \gamma + 1) \quad (1)$$

$$\beta = 180° - 2\gamma \quad (2)$$

$$R = \sin (\gamma - \theta)/\sin (\gamma), \quad (3)$$

where θ is the dip of the fault, γ is the axial angle of the fault-bend fold, β is the dip of the forelimb and R is the change in slip across the fault-bend fold (Fig. 1). Recently, such models have been translated into velocity descriptions of deformation, allowing the combination of tectonic and sedimentary modelling (Hardy & Poblet 1995). This short note will present and apply a general method for quantifying the kinematics of fault-bend folding.

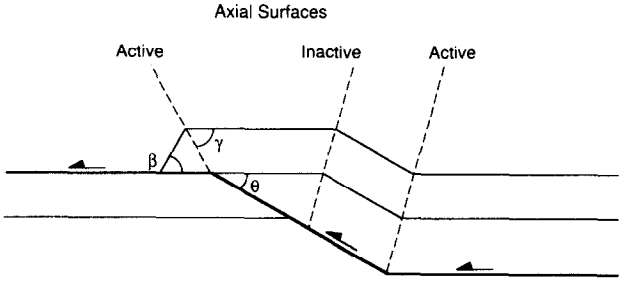

Fig. 1. The geometric model of fault-bend folding of Suppe (1983) for a simple step in décollement and the relationship of defined angles and axial surfaces.

THE VELOCITY DESCRIPTION OF DEFORMATION AND THE BLOCK CONTACT CONDITION

Waltham & Hardy (1995) presented the velocity description of deformation in some detail and velocity fields were derived for a range of geological processes (for example, pure shear, inclined or vertical simple shear, bulk rotation and compaction). The velocity description of deformation is applied here to hanging-wall deformation by layer parallel slip in which cross-sectional area is preserved. It was noted that the velocity fields derived for a given deformation mechanism cannot be entirely arbitrary and, in particular, they must: (a) conserve mass; and (b) not produce space problems. Where processes such as pore collapse, dissolution/precipitation and pressure solution are important, this approach may not be applicable. The first of these constraints requires that the velocities obey the continuity equation (Birkoff 1955):

$$\nabla \cdot (\rho \mathbf{v}) + \partial\rho/\partial t = 0, \quad (4)$$

where ρ is density, $\mathbf{v}$ is vector velocity and t is time. If density is assumed to remain constant, this equation reduces to:

$$\nabla \cdot \mathbf{v} = 0. \quad (5)$$

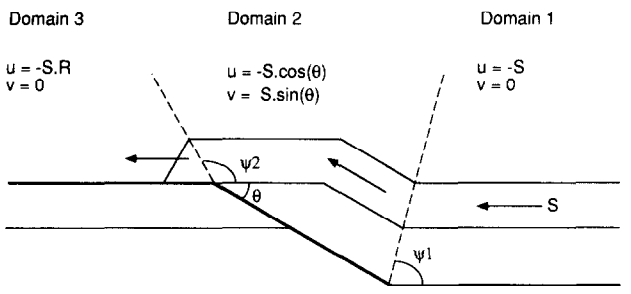

Fig. 2. The velocity model of fault-bend folding of Hardy & Poblet (1995), showing the horizontal and vertical velocities in the three velocity domains, and the angles ψ_1 and ψ_2. S is the slip rate, R is the reduction in slip across the fault-bend fold, and u and v are the horizontal and vertical velocities, respectively.

For two-dimensional processes (assuming conservation of cross-sectional area), the relevant equation is:

$$\partial u/\partial x + \partial v/\partial y = 0, \quad (6)$$

where u and v are the horizontal and vertical velocities respectively.

Waltham & Hardy (1995) showed that a further constraint on possible velocity fields applies when there is a series of distinct regions, each of which is governed by different velocity equations. These regions may be distinct fault blocks, or they may be different velocity regions above a fault-fold structure (Fig. 2). The constraint is that adjacent blocks or regions should remain in contact at all times with no gaps appearing between them and no overlapping areas. Waltham & Hardy (1995) showed that this contact condition required that, at all points along a fault or a velocity boundary, $f(x)$:

$$v_1 - u_1 \cdot \partial f/\partial x = v_2 - u_2 \cdot \partial f/\partial x, \quad (7)$$

where v_1 and u_1 are velocities for the block or region to be left, and v_2 and u_2 are velocities for the block or region to the right, of the boundary.

APPLICATION TO THE KINEMATICS OF FAULT-BEND FOLDING

Equations (6) and (7) can be used to investigate the kinematics of fault-bend folding, initially for the case of a simple step in décollement (Fig. 1). In this geometric model, displacement is parallel to the local fault orientation and the fold grows as a result of kink-band migration (Suppe 1983). This leads to three distinct velocity domains above the thrust (Fig. 2). In Domain 1, displacement is parallel to the lower décollement; in Domain 2, displacement is parallel to the ramping fault plane and in Domain 3, displacement is parallel to the upper décollement. Slip is conserved between Domains 1 and 2, but is consumed across the boundary between Domains 2 and 3. The horizontal (u) and vertical (v) velocities in the three domains are given by (Hardy & Poblet 1995):

$$\text{Domain 1} \quad u = -S \quad (8)$$

$$v = 0 \quad (9)$$

$$\text{Domain 2} \quad u = -S \cdot \cos(\theta) \quad (10)$$

$$v = S \cdot \sin(\theta) \quad (11)$$

$$\text{Domain 3} \quad u = -R \cdot S \quad (12)$$

$$v = 0, \quad (13)$$

where S is the slip rate (m ka^{-1}), θ is the thrust ramp angle and R is the reduction in slip across the fault-bend fold (equation 3). As the horizontal and vertical velocities within each domain are constant, the continuity condition (equation 6) is clearly satisfied. The necessary orientations (ψ_1 and ψ_2) of the boundaries between the domains can now be derived by substituting the relevant velocities into equation (7). For domains 1 and 2, this gives:

$$S \cdot \sin(\theta) + S \cdot \cos(\theta) \cdot \partial f/\partial x = S \cdot \partial f/\partial x \quad (14)$$

which, rearranging, gives:

$$\partial f/\partial x = \sin(\theta)/(1 - \cos(\theta)). \quad (15)$$

For $\theta = 30°$, equation (15) predicts that the velocity boundary (f) between Domains 1 and 2 must be inclined at an angle, ψ_1 of 75°, which is the bisector of the lower bend in the decollement (cf. Suppe 1983). Secondly, equation (7) can be used to derive any changes in slip (R) necessary between Domains 2 and 3, given the inclination (ψ_2) of the boundary between them. Substituting the velocities from Domains 2 and 3 into equation (7) gives:

$$R \cdot S \cdot \partial f/\partial x = S \cdot \sin(\theta) + S \cdot \cos(\theta) \cdot \partial f/\partial x \quad (16)$$

which, rearranging, gives:

$$R = \sin(\theta)/(\partial f/\partial x) + \cos(\theta). \quad (17)$$

When the boundary is that given by Suppe's equations for a ramp dipping at 30°, i.e. $\gamma = 60°$ or $\psi_2 = 120°$, equation (17) predicts a slip ratio (R) of 0.577, which is identical to that predicted by equation (3). Indeed, the fault-bend fold model of Suppe (1983) is just a specific instance, which preserves both line length and bed thickness, of this more general kinematic model.

The power of the approach described here is that, for an arbitrary inclination of the upper velocity boundary, the method predicts the change in slip necessary across it. Slip ratios for a range of boundary inclinations (ψ_2) are shown in Fig. 3 for a ramp dipping at 30°. From Fig. 3 it can be seen that, for values of ψ_2 less than 75°, an increase in slip is required across the boundary, while for values greater than 75°, a decrease in slip is required. Note that when ψ_2 is 150°, the change in slip is zero, as this is the condition of displacement parallel to the velocity boundary resulting in a through-going thrust with no bend in the detachment.

The method also applies to more complex, high-angle, reverse faults such as that illustrated in Fig. 4. Figure 4(a) shows a model of hangingwall deformation in which slip rate parallel to the fault segments is con-

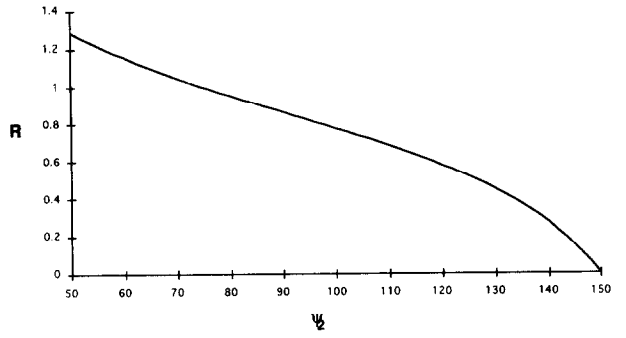

Fig. 3. Graph showing the slip ratios (R) necessary for a range of orientations of the velocity boundary between the ramp and upper décollement (ψ_2) for the case of a simple step in décollement fault-bend fold with $\theta = 30°$.

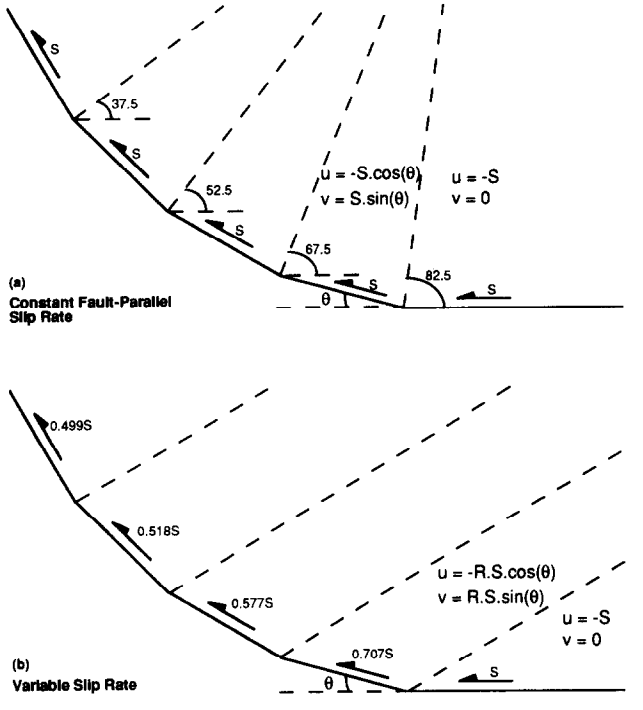

Fig. 4. Models of fault-bend folding in the hangingwall of a segmented reverse fault whose dip decreases from 60 to 0° by 15° across each fault segment. (a) Slip is constant parallel to the fault and is conserved across each axial surface. (b) Slip is imposed on the bottom fault segment and is consumed across each active axial surface. Horizontal and vertical velocities are shown for the first two domains in each case.

stant and conserved across each active axial surface. The block contact condition (equation 7) has been applied to determine the orientation of each of the velocity boundaries ensuring that area is conserved in the hangingwall. In contrast, in Fig. 4(b), displacement is imposed (specified) on the lowest fault segment and propagated upwards through the hangingwall and across each of the active axial surfaces which dip at 30°. As the velocities in the lowest segment and the orientation of all the active axial surfaces are known, equation (7) allows the velocities and resultant slip rate in each domain to be calculated sequentially from right to left through the hangingwall. For the case illustrated in Fig. 4(b), this analysis indicates that the slip parallel to the fault must decrease from S in the lowest domain to $0.499S$ in the uppermost domain. In fact, the horizontal and vertical velocities within each domain are identical to those predicted by inclined simple shear (60° antithetically) (cf. Waltham & Hardy 1995).

The faults in Fig. 4 could also be treated as extensional structures and the kinematics of hangingwall deformation associated with extensional faulting analysed. Extensional displacement (from left to right) requires that the horizontal and vertical velocities within each of the domains in Fig. 4 change sign compared to the velocities under compression. If equation (7) is then applied as before, the derived orientations of axial surfaces and changes in slip rate are identical to those for compression, but with a different sense of movement. More complex geometries, such as ramp-flat structures, could also be treated in this manner.

Thus the approach allows both the necessary orientations of active axial surfaces (when slip is specified) and changes in slip (when active axial surfaces are specified) to be derived for a given model of hangingwall deformation. Geometric and kinematic models can be checked easily for area conservation in this manner. However, some caution must be used when applying equation (7), as while it ensures the kinematic admissibility of a given model, it says nothing with regard to its geological plausibility. Therefore, care must be taken to ensure that the deformation mechanism implicit in the derived kinematic model is compatible with the geologic setting under consideration.

CONCLUSIONS

This short note has shown the applicability of the velocity description of deformation and the block contact condition (Waltham 1992, Waltham & Hardy 1995) to the kinematics of compressional fault-bend folding. The power of this approach is that it encompasses previous geometric approaches (giving identical results), but allows the kinematic consequences of a range of orientations of velocity boundaries (active axial surfaces) to be quantified. Complex, high-angle, fault-bend fold kinematics, and hangingwall deformation associated with extensional faults, may also be quantified using this method. The derived velocities can then be used in simple mathematical models to test the geometric consequences of such differences in kinematics (cf. Hardy & Poblet 1995).

Acknowledgements—Thanks to Dave Waltham and Josep Poblet for many discussions on this topic and to Craig Docherty for reading an earlier version of this note. The constructive comments made by reviewers Don Medwedeff and David Ferrill significantly improved this paper. The receipt of a Royal Society European Science Exchange Post-Doctoral Fellowship is gratefully acknowledged.

REFERENCES

Birkoff, G. 1955. *Hydrodynamics*. Dover Publications, New York.

Hardy, S. & Poblet, J. 1995. The velocity description of deformation. Paper 2: Sediment geometries associated with fault-bend and fault-propagation-folds. *Mar. Petrol. Geol.* **12**, 165–176.

Rich, J. L. 1934. Mechanics of low-angle overthrust faulting as illustrated by the Cumberland Thrust Block, Virginia, Kentucky and Tennessee. *Bull. Am. Ass. Petrol. Geol.* **18**, 1584–1596.

Suppe, J. 1983. Geometry and kinematics of fault-bend folding. *Am. J. Sci.* **283**, 684–721.

Suppe, J., Chou, G. T. & Hook, S. C. 1991. Rates of folding and faulting determined from growth strata. In: *Thrust Tectonics* (edited by McClay, K. R.). Chapman & Hall, 105–121.

Waltham, D. 1992. Mathematical modelling of sedimentary basin processes. *Mar. Petrol. Geol.* **9**, 265–273.

Waltham, D. & Hardy, S. 1995. The velocity description of deformation. Paper 1: Theory. *Mar. Petrol. Geol.* **12**, 153–164.

Zoetemeijer, R., Sassi, W., Roure, F. & Cloetingh, S. 1992. Stratigraphic and kinematic modeling of thrust evolution, northern Apennines, Italy. *Geology*, **20**, 1035–1038.